Journal of Radioanalytical and Nuclear Chemistry
https://doi.org/10.1007/s10967-025-10429-z

Dosimetric evaluation using EPR/alanine and radiochromic film detectors in end-to-end brain stereotactic radiosurgery sessions

Salvatore Panzeca[1] · Alvaro de Farias Soares[2,3] · Giuseppina Iacoviello[4] · Teresa Cucchiara[5] · Salvatore Gallo[6] · Mattia Romeo[2,3,7] · Maria Cristina D'Oca[2,3,8] · Maurizio Marrale[2,3,8]

Received: 16 July 2025 / Accepted: 23 September 2025

Abstract
This pilot study aimed to establish end-to-end stereotactic radiosurgery (SRS) sessions and evaluate the accuracy of the delivered doses using EPR/alanine and GAFChromic™ EBT3 films. Six Planning Treatment Volumes (PTVs), representing variations in tumor size, location, and proximity to Organs at Risk (OARs), were assessed using an anthropomorphic male head phantom irradiated with a TomoTherapy Hi-Art system (fraction of 10.5 Gy). Maximum deviations ranged from − 0.35 to 0.16 Gy, and − 0.35 to − 0.08 Gy, for alanine and films, respectively, even under complex spatial dose distribution (e.g., PTV6). Therefore, the findings demonstrated the reliability of both systems for precise SRS dosimetry.

Keywords Alanine · Cranial stereotactic radiosurgery · End-to-end test · Radiochromic films

Introduction

Despite the improvements in tumor treatment, brain metastasis (BM) constitutes an important source of mortality and accounts for around 20% of patients with systemic cancer. BMs are mostly associated with the spread of tumors originating from the breast, lung, kidneys, and melanoma [1]. Among the treatment options for BM patients, one can mention chemotherapy, surgery, and radiotherapy. Nowadays, treatment strategies are in steady development, including advancements in dose delivery. Whole-brain radiotherapy (WBRT), for example, has been an adopted option for patients who have multiple brain metastases [2, 3], while stereotactic radiosurgery (SRS) has allowed for obtaining a good localized tumor control [4–6].

SRS delivers extremely localized irradiation, allowing for reaching high absorbed doses to well-defined target volumes, while sparing the surrounding and non-target areas. The decline in cognitive function, for example, proved to be less frequent among SRS-treated patients than those treated with WBRT, without decreasing overall survival. It has resulted in an increase in SRS treatments as a precise and effective alternative [7, 8]. The Gamma Knife is an example of SRS, which is mostly performed using a single dose fraction. In case of large tumors, though,

✉ Alvaro de Farias Soares
alvaro.defariassoares@unipa.it

✉ Maurizio Marrale
maurizio.marrale@unipa.it

1 Azienda Sanitaria Provinciale Palermo, Via Giacomo Cusmano, 24, 90141 Palermo, Italy

2 Department of Physics and Chemistry "Emilio Segrè", University of Palermo, Viale Delle Scienze, Edificio 18, 90128 Palermo, Italy

3 Catania Division, National Institute for Nuclear Physics (INFN), Via Santa Sofia, 64, 95123 Catania, Italy

4 Health Physics Division-A.R.N.A.S. Palermo Civic Hospital, Piazza Nicola Leotta, 4, 90128 Palermo, Italy

5 Radiation Therapy Division-R.N.A.S. Palermo Civic Hospital, Piazza Nicola Leotta, 4, 90128 Palermo, Italy

6 Department of Physics and Astronomy "Ettore Majorana", University of Catania, Via Santa Sofia, 64, 95123 Catania, Italy

7 Department of Biological, Chemical and Pharmaceutical Sciences and Technologies, University of Palermo, Viale Delle Scienze, Edificio 16, 90128 Palermo, Italy

8 Advanced Technologies Network Center, University of Palermo, Viale Delle Scienze, Edificio 18a, 90128 Palermo, Italy

Published online: 24 October 2025

hypofractionated stereotactic radiotherapy (SRT) may be more appropriate due to its radiobiological advantages [9].

Still in the scope of SRS, intensity-modulated radiation therapy (IMRT) has demonstrated excellent target coverage with highly conformal doses and sparing of organs at risk (OAR), as observed in head and prostate cancer [10–12]. Helical TomoTherapy (HT), a modality of IMRT, performs a 3D conformal dose delivery. To achieve it, the beams are both spatially and temporally modulated, maximizing the dose to the tumor and minimizing the dose to healthy tissues. IMRT with HT may differ from other stereotactic techniques because the planning and treatment plans are not associated with a coordinate system, although HT would also provide an accurate image-guided procedure. Moreover, the use of non-invasive immobilization devices allows for the use of hypofractionation [13].

These different developments in radiotherapy have posed challenges for dosimetry, including the use of small fields or the introduction of techniques that dynamically change the radiation beam during treatment [14] (as is the case with IMRT). Additionally, there is increasing awareness of the exposure of healthy tissues to low doses and the associated risks of secondary tumor induction. Therefore, accuracy in dosimetry is important not only from an optimization point of view but also for data generation that can improve future radiotherapy treatments [15].

Given these new challenges introduced in the dosimetry area, studies assessing dose delivery in SRS have been recently reported, using different detection systems, including alanine, GAFChromic™ films [16–22] and diamond detectors [23]. Other dosimeters, based on luminescence, have also been investigated. For example, Elter et al. [24] performed an end-to-end test of an MRgRT treatment using a pelvis phantom ADAM-PETer (positron emission tomography (PET) Extension for Radiotherapy), in which thermoluminescence detectors (TLDs) were used for estimating the doses delivered. Deviations up to -4.7% were reported for the surface of the prostate. According to the authors, this deviation would be associated with small positioning uncertainties due to the gradient or related to the calibration process. Furuya et al. [25] evaluated the potential use of radiophotoluminescence dosimeters (RPLDs) to estimate the dose in stereotactic body radiation therapy (SBRT), in a post-operative spine case, finding similar accuracy values (within ± 5%). For means of comparison, for diamond detectors, slightly lower uncertainties (up to 4%) have been reported [23].

As for the studies that used alanine as the main detection system in SRS, there are a few reports on assessing quality control in the specific context of volume modulated arc technique (VMAT), using either homogeneous or heterogeneous phantoms, but usually for a single treatment scenario [17, 21]. Uncertainty values were found within 5% for a 95% confidence level [17].

Therefore, this study aimed to evaluate the accuracy of dose delivery in SRS sessions by non-conventional radiotherapy equipment, namely the TomoTherapy Hi-Art System. This is performed as a pilot study to assess the viability of the method. The adoption of an end-to-end test is to analyze that the entire sequence of radiation treatment, from CT imaging to beam delivery, is appropriately implemented and ensures sufficient accuracy in the delivery of the planned dose. Various tumor sizes, locations, and numbers of lesions were considered in order to evaluate the robustness of the procedure.

The dosimetric system used in this work is based on Electron Paramagnetic Resonance (EPR) alanine [26–31], and its response is compared to that of GAFChromic™ films. The films are specially designed for two-dimensional dose evaluation and provide accurate measurements of dose distribution and absorption gradients. The use of alanine relies on its stable signal after irradiation and a non-destructive readout. Furthermore, alanine detectors display a linear dose–response curve up to high dose levels of about 10^5 Gy and are dose-rate independent within the range used in SRS [32]. This approach allows for a comprehensive assessment of the method's robustness across clinically relevant scenarios.

Materials and methods

Irradiation treatment equipment

The SRS procedures were performed with a TomoTherapy Hi-Art system (Accuray, Madison, WI, USA) installed at the U.O. of Radiotherapy of the Civic Hospital of Palermo (Palermo, Italy). This system integrates treatment planning, an Image Guided Radiation Therapy (IGRT), and the hardware system administration of the dose. This treatment modality has a differential of continuously rotating around the patient, delivering doses in a helical reference [33].

Phantom

An anthropomorphic RANDO-Alderson male head phantom (The Phantom Laboratory, Greenwich, NY, USA) was used in all irradiation procedures [34]. The phantom consists of a skull embedded in soft-tissue-equivalent material according to ICRU standards (report no. 44) [35], which reproduces the attenuation and scattering conditions found in a human head. The phantom is composed of 25-mm-thick layers, where films can be placed between them. Each layer has a grid (dimension of 3 cm × 3 cm) of holes (5-mm diameter each) filled with detachable plugs for alanine dosimeter

placements. This configuration enables flexible and reproducible placement of detectors in different anatomical regions, thereby allowing detailed three-dimensional dose mapping.

Dosimeters

EPR measurements were obtained with alanine pellets produced by Gamma-Service Produktbestrahlung GmbH (Leipzig, Germany), having dimensions of 4.8 ± 0.2 mm in diameter and 2.99 ± 0.10 mm in height.

The films employed in this work were GAFChromic™ EBT3 (batch number 11031502205) ones, having sheet dimensions of about $20.3 \times 25.4\,cm^2$ (Ashland ISP Advanced Materials, NJ, USA).

Alanine dosimeter calibration and irradiation procedures

For each irradiation dose in the calibration curve, three alanine dosimeters were placed inside one of the cylindrical housings (0.6 cm diameter each) of a Cheese Phantom (Eastman Kodak Co., Rochester, NY, USA). The housing was located 0.5 cm below the phantom's midplane along its vertical axis. The phantom containing alanine dosimeters was irradiated with a 6 MV X-ray beam from a dual-energy Varian DHX-S LINAC (Varian Medical Systems, Palo Alto, CA) equipped with a Millennium 120-leaf MLC. The field size was $10 \times 10\,cm^2$, and doses varied in the range of 1–25 Gy.

Radiochromic film calibration and irradiation procedures

Films were placed into a phantom made of $30 \times 30\,cm^2$ sheets (1 cm thick each) of solid water from PTW (Freiburg, Germany), plus 10 cm of the buildup material above the film (for constant backscattering conditions). An 85 cm source-to-film distance was adopted. Film samples were cut into equal pieces of $3.0 \times 3.0\ cm^2$ and irradiated perpendicularly to the 6 MV beam. The radiation was performed with the same machine as used for the alanine-pellets irradiation, and using the same field size. An Exradin A1-SL calibrated ion chamber (Standard Imaging, Inc., Middleton, WI, USA) was inserted below the film to verify the LINAC output during the irradiation. For the calibration curve, films were irradiated with different doses up to 25 Gy.

The LINAC was calibrated following the IAEA TRS-398 code of practice [36], with an ionization chamber Farmer-type model 30,013 from PTW (Freiburg, Germany). The chamber was placed in a water phantom (10 cm in depth). A source-to-surface distance of 100 cm and a 10 cm × 10 cm field were used for all procedures.

EPR measurements

EPR measurements were carried out at constant temperature (25 ± 1 °C), using an ELEXSYS E580 spectrometer from Bruker (Rheinstetten, Germany) operating at the X-band (average frequency of 9.7 GHz). The EPR spectra were acquired using a microwave power of 3.00 mW and a modulation amplitude of 10 G.

The pellets were read out considering four orientations within the resonating cavity to account for potential anisotropic effects. Each measured peak-to-peak amplitude (H_{pp}) of the central line of the EPR spectrum of alanine was normalized by the mass. For each dose value, three dosimeters were irradiated, and the mean value of all 12 H_{pp} measurements (four orientations × three dosimeters) was taken as the dosimetric output signal [37]. The H_{pp} standard deviation was always within $\pm 3\%$.

Scanning analysis

An Epson scanner model Expression 10000XL (Seiko Epson Corp., Nagano, Japan), and its software (EPSON SCAN v3.49) were used to read the films. Raw images obtained from the films were imported into the Physics Analysis Workstation, which is integrated into the computer system of TomoTherapy using FILM Analyzer software (Radiological Imaging Technology, Inc., CO) for image processing. The signal obtained by each channel was converted to a net optical density (OD), and the sensitometric curve was calculated, as reported in the literature [38, 39].

The dose received by the film at 1.5 cm was calculated from the dose measured at 10 cm, using the depth-in-water performance curve of the beam. In particular, the dose value received from each element $D_{w,Q}$ was calculated as follows:

$$D_{w,Q} = M \times k_{TP} \times k_s \times k_{pol} \times k_{elec} \times N_{D,w,Q}$$

where M is the reading of the electrometer; k_{TP} is the correction factor for temperature and pressure considering the difference of the ambient conditions of measurement with respect to the ambient conditions of calibration of the ionization chamber; k_s is the correction factor for ion recombination; k_{pol} is the correction factor for the voltage polarity effect; k_{elec} is the correction factor that takes into account the sensitivity of the electrometer; $N_{D,w,Q}$ is the calibration coefficient of the chamber in absorbed dose in water for a radiation quality Q [36, 40].

Treatment plans simulation

CT scans of the RANDO Head Phantom were used to simulate six different clinical situations regarding “tumor”

dimension, position, and proximity relations with OAR. To make the positioning reproducible, the RANDO Head Phantom was placed on a headrest and subsequently used for all irradiations. Furthermore, to minimize repositioning errors during irradiation and to uniquely identify a spatial reference system (necessary for the dose calculation system), 3 metal marks were positioned on the external surface of the RANDO-phantom, one on the forehead and two on the ears (one on each side), to identify a single axial plane.

For having centering CT parameters like those used in clinical practice, a voltage of 120 kV and 25 mm thick slices were set. Target volumes and healthy structures were delimited by the Pinnacle^3 workstation (Hitachi Medical Corporation, Tokyo, Japan). During the treatment delivery, alanine dosimeters were placed in the phantom housings to estimate the delivered doses by the PTV (Planning Treatment Volume) and OAR. GAFChromic™ films were inserted between contiguous slices of the phantom to obtain the bidimensional dose distributions. For all PTVs, the treatment plan simulates 1 fraction of treatment delivering a dose of 10.5 Gy. In Table 1, for each PTV, details on the localization of the lesion, the Clinical Target Volume (CTV), the maximum dimensions (H × W) in the transverse, sagittal, and coronal planes, along with other treatment parameters, are shown.

Planning treatment volume

Figure 1 shows the transversal, sagittal and coronal views of the lesions under examination for the different PTVs. For PTV6, three lesions can be observed (Fig. 1f). In the supplementary material, the setups and contour maps for each of the PTVs, as well as the DVH (Dose Volume Histogram) and DQA (Delivery Quality Assurance) analyses of both PTV and OAR, are available (Figures S1 and S2 in the supplementary material).

During PTV deliveries 1 and 2, the alanine pellets were placed in slice 3 and the GAFChromic™ film was inserted between contiguous slices 3 and 4 of the phantom. For PTVs 3 and 4, alanine pellets were placed in slice 1 and the GAFChromic™ film was inserted between slices 0 and 1. In case 5, alanine dosimeters were placed in slice 2, and the GAFChromic™ film was inserted between slices 2 and 3. Finally, in the case of PTV number 6, the setup was given by alanine dosimeters in slice 3 and two GAFChromic™ films between contiguous slices 3–4 and 4–5 of the phantom. Two films were used, as the latter PTV had three lesions (Fig. 1f).

Results

Alanine dosimeter calibration

Figure 2 shows the calibration curve of alanine dosimeters irradiated in the range of 1–25 Gy. The error bars correspond to the standard deviation of the signal of three samples, each of them being measured in four directions within the cavity and normalized by the mass [37, 41].

The dose–response curve follows a linear trend. The experimental data were fitted with the following function:

$$h = b * D + A$$

where the *b* value corresponds to dosimetric sensitivity, *D* is the irradiation dose and *A* is a constant. Table 2 presents the fitting results, in which an R^2 of 0.99997 was obtained, indicating a good agreement between experimental and theoretical data.

Uncertainty related to alanine readout was considered as 1.4% (k = 2), and the batch reproducibility as 1% (k = 2) [42].

Radiochromic film calibration

Figure 3 shows the calibration curve of radiochromic films irradiated in the range of 1–25 Gy. The curve has an exponential increase, which starts to saturate for doses above

Table 1 Parameters used for PTV and OAR measurements

PTV	Number of lesions	Lesion region	CTV (cm^3)	Maximum dimensions (H × W) planes (cm)			Field width (FW)	Pitch	Modulation factor
				Transverse	Sagittal	Coronal			
1	1	Right temporal	3.50	1.70 × 1.80	2.15 × 1.75	2.4 × 2.00	1.0	0.172	2.00
2	1	Right temporo-Cerebellar	6.33	2.20 × 2.20	2.22 × 2.25	2.30 × 2.35	2.5	0.172	2.00
3	1	Right frontal(Not OAR)	1.79	1.35 × 1.55	2.10 × 1.30	2.10 × 1.70	1.0	0.215	1.60
4	1	Left parieto-occipital	1.79	1.70 × 1.60	1.80 × 1.70	1.80 × 1.65	1.0	0.215	2.00
5	1	Right temporal	3.61	2.45 × 1.70	2.35 × 2.35	2.30 × 1.70	1.0	0.215	2.00
6	3	Left Front-Temporal	11.80	2.60 × 3.78	2.56 × 2.50	2.05 × 1.60	2.5	0.215	2.00
		Left cerebellar		1.70 × 1.90	1.20 × 1.80	1.35 × 1.25			
		Right cerebellar		1.20 × 1.45	2.30 × 1.70	1.20 × 1.80			

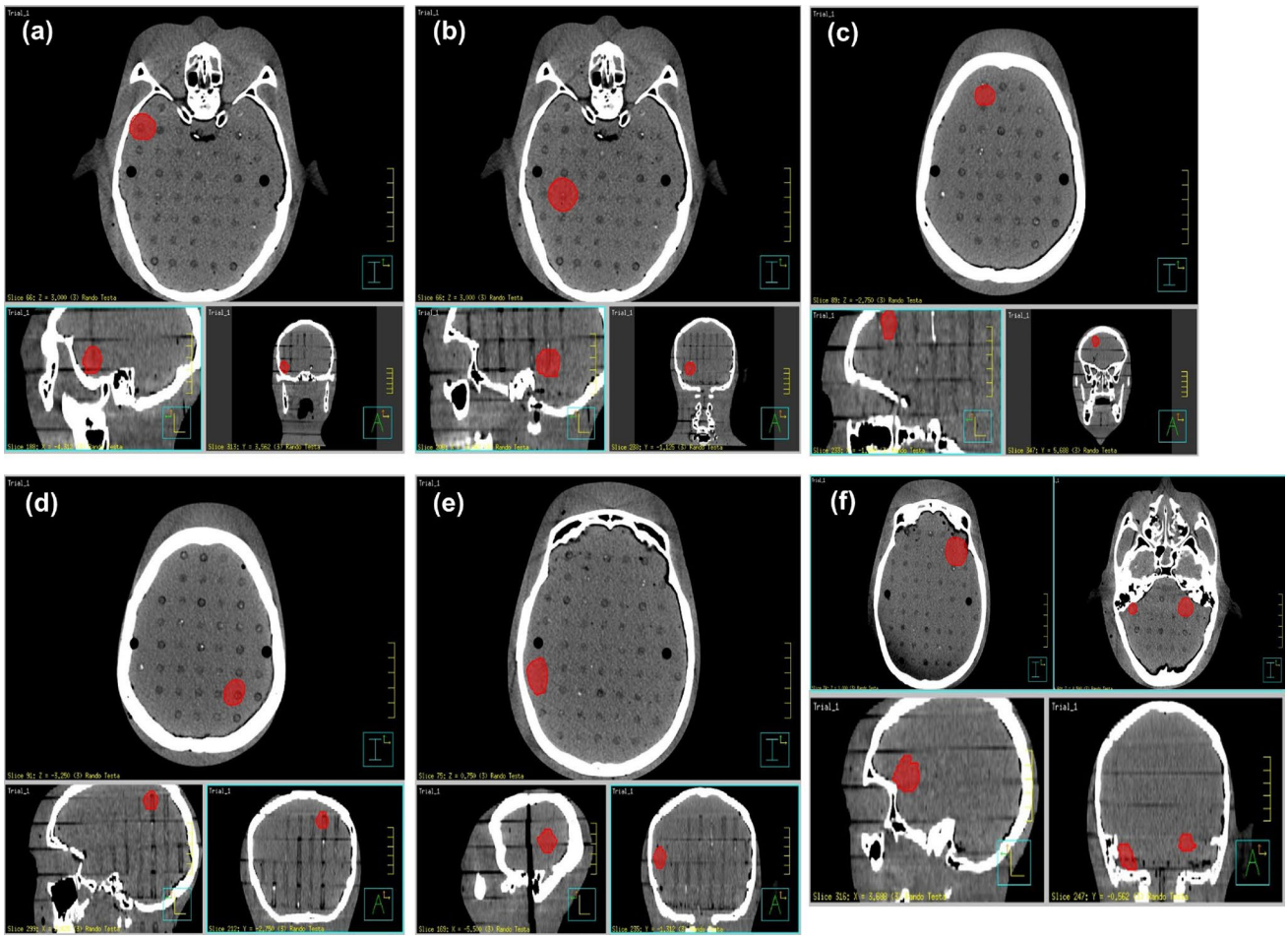

Fig. 1 Setup for (**a**) PTV1, (**b**) PTV2, (**c**) PTV3, (**d**) PTV4, (**e**) PTV5 and (f) PTV6, showing the transversal, sagittal and coronal views of the lesion under examination

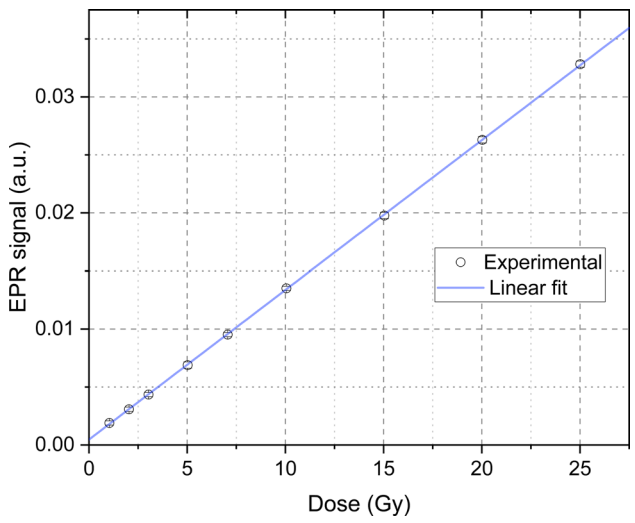

Fig. 2 Calibration curve of alanine irradiated in TomoTherapy with doses between 1 and 25 Gy

Table 2 Linear regression parameters as a function of EPR signal amplitude

Dosimeter	b (sensitivity) [$\times 10^{-3}$]	A [$\times 10^{-4}$]	R^2
Alanine *synergy health*	1.289 ± 0.003	5.0 ± 0.4	0.99997

5 Gy. This saturation becomes more pronounced for doses above 15 Gy. This dose–response curve behavior, with a saturation trend for doses above 10 Gy, is expected for this type of film, as already reported in the literature [22].

The dose received by the film at 1.5 cm was calculated from the dose measured at 10 cm, using the depth-in-water performance curve of the beam. The obtained curve was used in the DQA (Delivery Quality Assurance) station software platform to measure the dose imparted to the films during irradiation for the dosimetric verification of the calculated dose distributions.

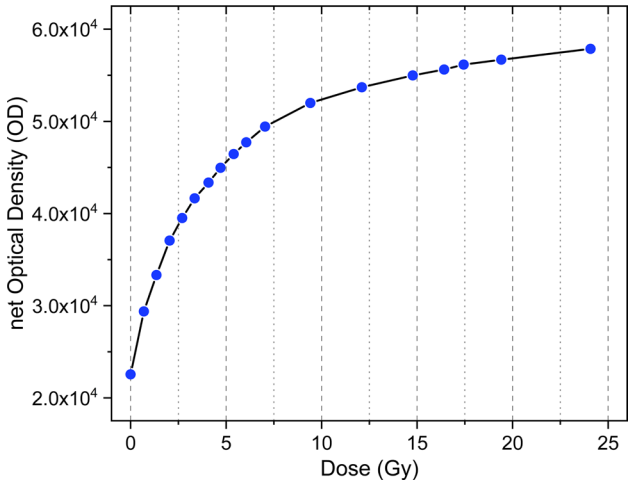

Fig. 3 Calibration curve of GAFChromic™ Films irradiated in TomoTherapy with doses between 1 and 25 Gy

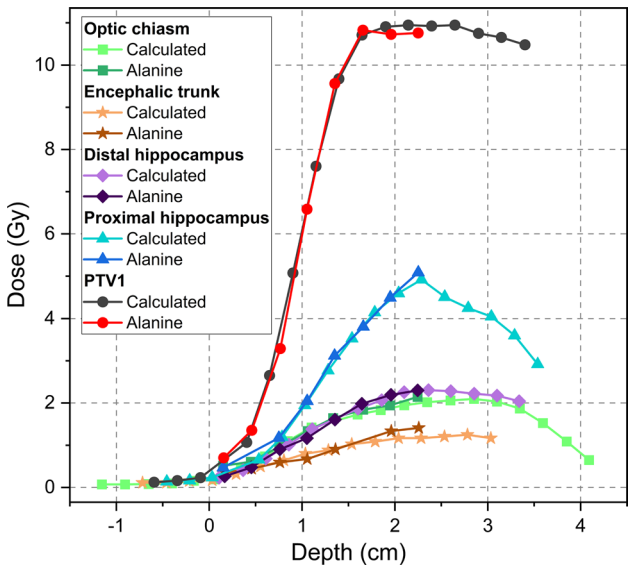

Fig. 4 Measured dose with alanine and calculated dose with DQA Plan for PTV1. From the analysis of the experimental data, the difference between the two data series was calculated

Accuracy of the dose delivered to PTV1

Once the calibration curves for both dosimetric systems were established, it was possible to use them to estimate the absorbed doses and their accuracy for each of the PTVs investigated in this study. Figures 4 and 5 show the comparison between the calculated and measured doses for PTV1 by EPR and GAFChromic™ film, respectively. It shows a good agreement between the doses measured with both systems, alanine and GAFChromic™, and those calculated with TomoTherapy TPS. In the case of the alanine curves, the doses are covered in a narrower range because of the experimental setup.

It is also worth noting that the agreement was observed not only for the PTV curves but also for the individual cases of optic chiasm, encephalic trunk, and hippocampus.

The maximum deviations (calculated dose minus the dose measured with alanine and films) for PTV1, and their respective OARs defined in this plan are listed in Table 3. The closest values of dose to the reference were obtained for the distal hippocampus and encephalic trunk for EPR and film measurements, respectively. Considering the maximum values of absorbed dose according to alanine measurements, variations were no higher than 0.20 Gy (around 2% of the treatment dose used, i.e., 10.5 Gy).

Accuracy of the dose delivered to PTV2

The agreement between the dose measured with alanine and with GAFChromic™ film, with the one calculated via TomoTherapy TPS, is shown in Figs. 6 and S3, respectively. As observed for PTV1, the results of measured and calculated doses were similar. Note that the curves obtained with films can be found in the supplementary material and are referred to throughout the text with the initial "S".

Table 3 has the maximum deviations for PTV2, and the respective OARs defined in this plan. Deviations were between − 0.30 and 0.19 Gy for alanine measurements.

Accuracy of the dose delivered to PTV3

Figure 7 shows the agreement between the doses measured with alanine and the calculated ones via TomoTherapy TPS. In the supplementary material, the same comparison is shown when using GAFChromic™ film (Figure S4). A good agreement was observed in both comparisons.

The maximum deviations for PTV3 and the OAR defined in this plan are 0.20 Gy with alanine and −0.20 Gy with films, in the constant dose area.

Accuracy of the dose delivered to PTV4

Concordance between the dose measured with alanine and with GAFChromic™ films and the calculated dose with TomoTherapy TPS is shown in Fig. 8 and Figure S4, respectively.

The maximum deviations for PTV4 and the OAR defined in this plan and based on the experimental data series are 0.20 Gy for alanine and −0.16 Gy for film in the constant dose area.

Fig. 5 Measured dose with film GAFChromic™ and calculated dose with DQA Plan for PTV1

Table 3 Maximum deviations (calculated dose minus dose measured with alanine and film) for PTV1, PTV2, PTV5, PTV6, and their respective OARs

Organ	Alanine		Film
	For the maximum measured dose (Gy)	For the minimum measured dose (Gy)	For the maximum measured dose (Gy)
	Area measurement – PTV1		
Proximal hippocampus	0.09	−0.17	−0.35
Distal hippocampus	−0.04	−0.32	−0.14
Optic chiasm	−0.14	−0.23	−0.35
Encephalic trunk	−0.20	0.13	−0.13
	Area measurement – PTV2		
Hippocampus	−0.20	−0.30	−0.08
Encephalic trunk	−0.15	0.19	−0.15
	Area measurement – PTV5		
Hippocampus	0.14	−0.11	−0.15
Encephalic trunk			−0.20
	Area measurement – PTV6		
Hippocampus	0.16	–	−0.19[1]
Encephalic trunk	−0.13	0.13	−0.16[1]/−0.22[2]

[1]Film 1. [2]Film 2

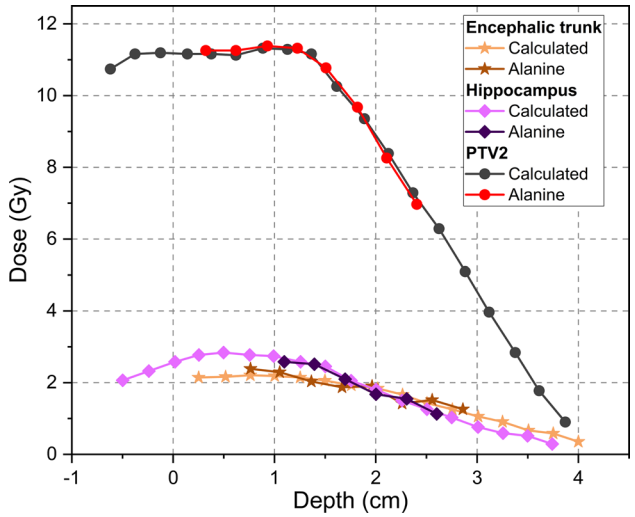

Fig. 6 Measured dose with alanine and calculated dose with DQA Plan for PTV2. From the analysis of the experimental data, the difference between the two data series was calculated

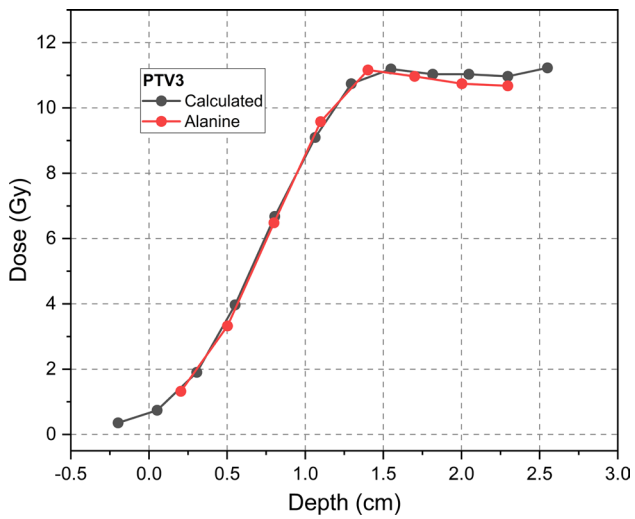

Fig. 7 Measured dose with alanine and calculated dose with DQA Plan for PTV3. From the analysis of the experimental data, the difference between the two data series was calculated

Accuracy of the dose delivered to PTV5

Figure 9 and Figure S6 show the agreement between the doses measured with alanine and GAFChromic™ films, in comparison to those from TomoTherapy TPS.

Table 3 shows the maximum deviations (calculated dose minus the measured dose) for PTV5 and for the OARs. Variations were within ± 0.20 Gy.

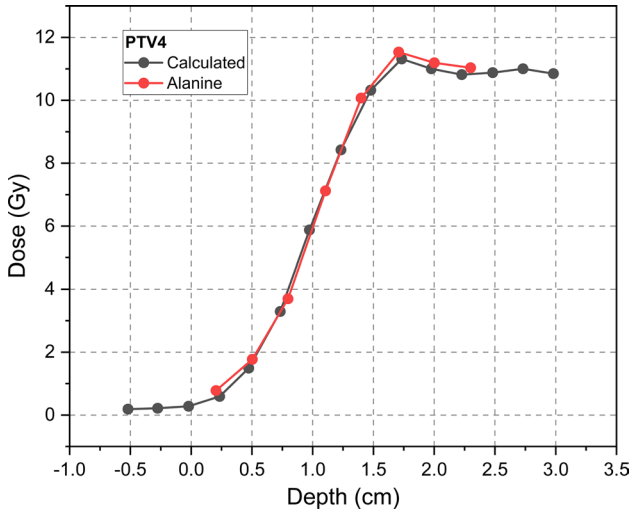

Fig. 8 Measured dose with alanine and calculated dose with DQA Plan for PTV4. From the analysis of the experimental data, the difference between the two data series was calculated

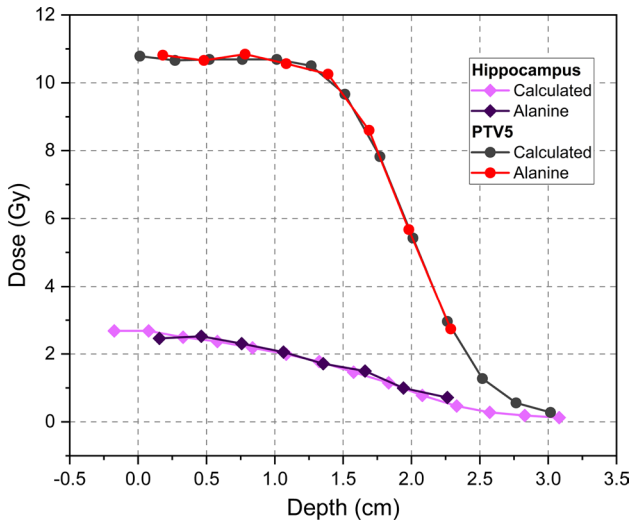

Fig. 9 Measured dose with alanine and calculated dose with DQA Plan for PTV5. From the analysis of the experimental data, the difference between the two data series was calculated

Accuracy of the dose delivered to PTV6

Figure 10 shows the curves comparing the doses measured with alanine and those calculated with TomoTherapy TPS. Figures S7, S8, and S9 depict a similar analysis performed with the films. As observed in the other PTVs, a good agreement between the experimental and calculated doses is found.

The maximum deviations for PTV6 and the OAR with PTV6 are shown in Table 3. A maximum variation of 0.16 Gy was found for alanine in the hippocampus case,

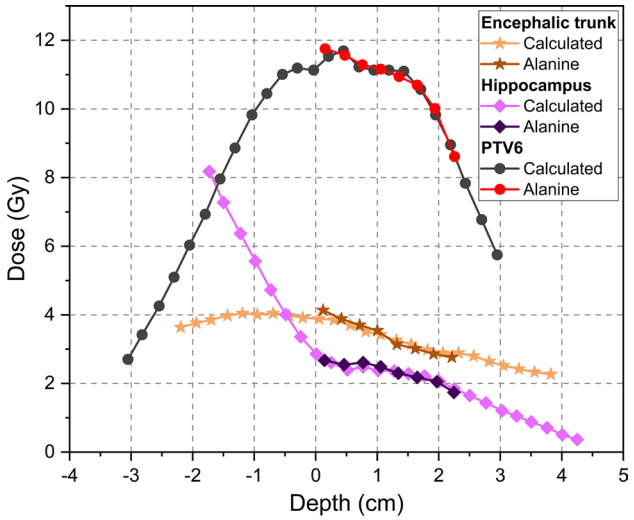

Fig. 10 Measured dose with alanine and calculated dose with DQA Plan for PTV6. From the analysis of the experimental data, the difference between the two data series was calculated

while for film, it was −0.22 Gy in the encephalic trunk case.

Discussion

In this work, successful end-to-end tests of SRS treatment by non-conventional radiotherapy equipment (TomoTherapy Hi-Art System) were performed using a RANDO Head Phantom. Dosimetric studies were carried out for the simultaneous treatment of multiple brain lesions with different shapes, sizes and positions using two independent measurement systems, alanine and GAFChromic™ films.

In Table 4, the measured doses for each PTV and OAR are summarized, showing that the dose constraints requested and set in TomoTherapy TPS have been most respected, except for the encephalon case, in which the maximum doses (D_{Max}) were slightly higher than the dose constraint ones (C).

The experimental results demonstrated that doses obtained using alanine dosimeters agreed with those calculated by the TomoTherapy TPS within the experimental error. This good agreement was observed in both PTV and OAR cases. It was the same even in the latter case, in which smaller doses were applied, proving that the EPR/alanine signal is reliable. Considering PTV5 as an example, data showed an excellent agreement between the calculated and measured doses not only for the PTV, which received a dose of 10.5 Gy per fraction, but also for the hippocampus, which received much lower doses, in the range between 1.5 and 2.5 Gy per fraction. These values are close to the minimum detectable dose (MDD) for alanine detectors. Similar considerations apply to the comparison between doses from the DQA module and those obtained with GAFChromic™ films. There is an excellent agreement, which is within the experimental error. Even in the most complex scenario in terms of spatial distribution, i.e., PTV6, the agreement remains. The 2D dose distribution of the films used for the PTV6 accurately follows the dose distribution calculated by the TPS.

Studies and audits of end-to-end tests have been extensively and successfully used in radiotherapy to validate the accumulated accuracy of all steps from pre-treatment imaging to dose delivery, in order to meet the safety standards of the treatment procedure involved, especially to validate new facilities or the entire chain of new treatment planning. However, for brain stereotactic surgery, this is less extensively reported.

Due to the alanine detector characteristics, such as its tissue equivalence, very stable post-irradiation signal and linear dose response, it has long been appreciated for dosimetric applications in radiotherapy [42], and therefore, studies on its use in SRS followed. The study of Albino et al. [21] used alanine for quality control of SRS. In their case, the treatment was performed by the VMAT, with a linear accelerator producing a 6 MV beam (at a flattening filter-free condition). But the scope of it was narrower than here, comprising only one treatment case with 4 lesions, irradiated with another modality, and using a single dosimetric system. In our approach, 6 different treatment plans were considered, one of them with multiple lesions. Additionally, two dosimetric systems were used, and the depth dose profile was investigated.

In another work of a similar context, Mazaro et al. [17], for example, characterized alanine detectors through dosimetric tests in VMAT to demonstrate their feasibility for quality control. The end-to-end test considered and simulated two different situations: homogeneous and heterogeneous. A strong linear correlation with dose was found ($R^2 = 0.99997$) for the calibration curve and insignificant dependence on dose rate. For a treatment planning dose of 18 Gy, results from alanine showed an uncertainty of 4.60% (95% confidence level). This represents a higher uncertainty than our results, despite the higher dose of 18 Gy, while 10.5 Gy was used here.

The agreement achieved here (maximum variations of around 2%, considering the total treatment dose) with the end-to-end test is similar to the reported results for cranial SRS in two other end-to-end dosimetry audits. Dimitriadis et al. [16] evaluated 33 single-fraction treatment plans, which were assessed at 30 centres using anthropomorphic head phantom STEEV (Stereotactic End-to-End Verification) with a single irregularly shaped target, ~ 8 cc, at 10 mm from the brainstem. Absolute doses were measured with EBT-XD films and alanine pellets inside both the target and

Table 4 Constraints and dose values for the PTVs and OARs, and the target (T) and constraint (C) doses according to TPS

Organ	D_{Max} (Gy)	D_{Min} (Gy)	D_{Median} (Gy)	$D_{Average}$ (Gy)	Stand. Dev	Vol. (cm^3)	Target (T)—Constraint (C) (Gy)
PTV1							
PTV1	22.91	19.82	21.85	21.80	0.42	3.43	(T) 21
Encephalon	22.91	0.02	0.14	0.96	2.32	1400.60	(C) 18
Encephalic trunk	3.57	0.07	1.70	1.54	0.91	28.12	(C) 12
Optic Chiasm	5.40	2.83	3.66	3.76	0.56	1.93	(C) 10
Hippocampus	7.10	0.09	0.62	1.27	1.57	6.96	(C) 8
PTV2							
PTV2	22.39	19.67	21.81	21.74	0.38	6.20	(T) 21
Encephalon	22.39	0.04	0.56	2.15	3.47	1400.60	(C) 18
Encephalic trunk	9.44	0.22	2.95	2.98	1.33	28.12	(C) 7
Optic Chiasm	3.58	1.86	2.57	2.63	0.38	1.93	(C) 10
Hippocampus	7.58	0.34	1.56	2.28	1.61	6.96	(C) 6
PTV3							
PTV3	22.23	20.59	21.62	21.60	0.31	1.71	(T) 21
Encephalon	22.23	0.02	0.14	1.13	2.42	1400.60	(C) 18
PTV4							
PTV4	22.04	20.81	21.49	21.47	0.23	2.02	(T) 21
Encephalon	22.04	0.02	0.11	1.17	2.62	1400.60	(C) 18
Encephalic trunk	0.11	0.01	0.05	0.05	0.02	28.12	(C) 7
Optic Chiasm	0.05	0.04	0.05	0.05	0.00	1.93	(C) 10
Hippocampus	0.30	0.05	0.09	0.11	0.06	6.96	(C) 6
PTV5							
PTV5	22.15	20.37	21.61	21.56	0.27	3.50	(T) 21
Encephalon	22.11	0.04	0.29	1.32	2.61	1400.60	(C) 18
Encephalic trunk	2.93	0.04	0.16	0.50	0.63	28.12	(C) 7
Optic Chiasm	0.30	0.11	0.15	0.16	0.05	1.93	(C) 10
Hippocampus	5.13	0.15	1.41	1.75	1.17	6.96	(C) 5
PTV6							
PTV6	22.86	19.55	22.00	21.90	0.45	11.23	(T) 21
Encephalon	22.86	0.13	3.45	4.46	4.19	1400.60	(C) 18
Encephalic Trunk	16.89	3.07	7.50	7.66	1.78	27.96	(C) 17
Optic Chiasm	7.79	4.16	5.04	5.14	0.54	1.93	(C) 10
Hippocampus	7.98	2.96	4.59	4.86	1.18	6.98	(C) 8

the brainstem and their responses were compared with the TPS-predicted ones. Comparison between the auditors and centers was within ± 2.4% of the dose determined by the TPS (range of 1.0% to + 2.4%). Carlino et al. [31] described an end-to-end test dosimetry audit implemented in a synchrotron-based pencil beam scanning (PBS) therapy facility. Three phantoms were used, one homogeneous and in-house produced and two anthropomorphic heterogeneous (head and pelvis). Doses obtained from 230 alanine pellets were compared to those from the Farmer ionization chamber in water. As a result, a systematic deviation of approximately 2% was found.

Mentioning other studies, which used film-based detection, there is the work of Hoffmans et al. [43], which investigated the usability of an anthropomorphic deformable and multimodal pelvis (ADAM-pelvis) phantom in combination with film dosimetry (GAFChromic™ EBT3 films) in an MR-guided RadioTherapy treatment (MRgRT) adaptive workflow. The delivered dose was evaluated at the interfaces of critical structures (e.g., bladder and rectum) by using small film pieces. Results corroborated with the dose calculations (based on electron density (ED) map using deformable image registration (DIR)-based and CT-based ED) and experimental film measurements, with average relative dose

differences < 3% for both calculated cases, which is quite close to the 3.3% found in our results.

In terms of PTV and effectively delivered doses, constraint and target values were most achieved, despite the complexity of the cases proposed. This good performance explains why SRS and SRT have taken the place of whole-brain irradiation in multiple brain metastases treatments, for example. However, variations at the millimeter level are found, which are important when dealing with either small tumors or at the margins of a PTV [44]. Therefore, ensuring the accuracy and safety of the treatment-delivered dose and its distribution are essential. This is even important before introducing new clinical techniques [43], and it needs to keep up with the new developments, in which a high dose may be delivered in a single fraction.

This context underscores the need for reliable dosimetric systems. The results reported here for different PTVs showed a maximum variation of 1.9% and 3.3%, for alanine and GAFChromic™ films, respectively, for a single dose fraction of 10.5 Gy. It corroborates previous studies [17, 31, 43], in which the reliability of alanine in SBRT and SRS contexts was attested. Moreover, this study is novel in evaluating six different PTVs and respective OARs, across different complexity scenarios, while comparing the response of two complementary dosimetric systems. These findings support the applicability of alanine and film-based dosimetry for quality assurance in complex SRS and SBRT treatments.

Comments on the limitations of the study

As a preliminary pilot investigation, the present study focused on brain tumors, analyzing clinical target volumes ranging from 1.79 to 11.80 cm^2 in both single- and multiple-lesion scenarios. Despite the heterogeneity in lesion size and spatial distribution, the results consistently demonstrated comparable levels of accuracy across all examined cases. Nevertheless, the restricted sample size (n = 6) constitutes a clear limitation, preventing statistically significant conclusions or broad generalizations. Expanding the study to a large cohort is therefore crucial, particularly to include patients with more complex or irregular geometries, such as multifocal tumors with non-uniform spacing or irregular margins, which are frequently encountered in clinical practice. Such an expansion would not only strengthen the validity of the approach but also provide deeper insights into its potential clinical applicability and robustness.

From a dosimetric perspective, the positioning of alanine pellets was constrained by the phantom configuration, which may have introduced systematic uncertainties in spatial localization. This emphasizes the importance of optimizing phantom design and detector placement to minimize geometric biases during experimental verification. Furthermore, as extensively reported in the literature, the use of alanine detectors can be particularly challenging at dose levels below 5 Gy, due to increased signal uncertainty [28, 45, 46]. This factor requires careful consideration, especially in stereotactic treatments or hypofractionated regimens, where low-dose regions adjacent to high-dose volumes are frequently present. Addressing these limitations will be essential for refining the methodology and ensuring its robustness in clinical practice.

Conclusion and future directions

This study presents end-to-end tests of stereotactic radiosurgery treatment using the TomoTherapy Hi-Art System. The RANDO Head Phantom was employed to simulate six distinct clinical scenarios, varying in tumor size, location, and proximity to Organs at Risk (OARs). Alanine dosimeters and GAFChromic™ films were utilized for dose measurement. The results demonstrated that the stereotactic cranial radiosurgery technique implemented with helical TomoTherapy achieves the high level of accuracy and precision required for such treatments. Additionally, alanine demonstrated strong potential for use in SRS quality control, particularly when used in combination with other detectors.

Further studies should address a large patient cohort, including cases with comparable or more complex lesion distributions. Incorporating alternative dosimetric systems with complementary sensitivity profiles, or adopting hybrid approaches that combine alanine with other detectors, would enhance measurement reliability across a broader dose range. Advanced computational modeling of dose distributions, validated against broad experimental datasets, could also help reduce uncertainties and support clinical implementation. Ultimately, expanding patient data, refining experimental design, and integrating multimodal dosimetric strategies will be essential to firmly establish the accuracy, reproducibility, and clinical relevance of this approach.

Supplementary Information The online version contains supplementary material available at https://doi.org/10.1007/s10967-025-10429-z.

Acknowledgements This work has received funding from the Italian Ministry of Research with the Project "SiciliAn MicronanOTecH Research And Innovation Center" SAMOTHRACE"(MUR,PNRR-M4C2, ECS_00000022), spoke5-Università degli Studi di Palermo "S2-COMMs—Micro and Nanotechnologies for Smart & Sustainable Communities" and by the European Union-NextGeneration EU, Mission 4 Component 2 Inv. 1.5 CUP B83C22003930001 "Tuscany Health Ecosystem (THE), Project" Development of Advanced dosimetric techniques for uLtra-hIgh dose rate beams (DALI').

Author contributions Conceptualization: *Giuseppina Iacoviello, Maurizio Marrale*; Methodology: *Salvatore Panzeca, Giuseppina Iacoviello, Teresa Cucchiara, Maria Cristina D'Oca*; Formal analysis and investigation: *Salvatore Panzeca, Alvaro de Farias Soares, Giuseppina Iacoviello*; Validation: *Alvaro de Farias Soares, Giuseppina Iacoviello, Maurizio Marrale*; Data Curation: *Salvatore Panzeca, Alvaro de Farias*

Soares, Maurizio Marrale; Writing—original draft preparation: *Salvatore Panzeca, Alvaro de Farias Soares, Salvatore Gallo, Maurizio Marrale*; Writing—review and editing*: Salvatore Panzeca, Alvaro de Farias Soares, Giuseppina Iacoviello, Teresa Cucchiara, Salvatore Gallo, Mattia Romeo, Maria Cristina D'Oca, Maurizio Marrale*; Resources: *Maurizio Marrale*; Supervision: *Maurizio Marrale*.

Funding Open access funding provided by Università degli Studi di Palermo within the CRUI-CARE Agreement.

Declarations

Conflict of interest The authors have no conflicts of interest to declare that are relevant to the content of this article.

References

1. Sacks P, Rahman M (2020) Epidemiology of brain metastases. Neurosurg Clin N Am 31:481–488
2. Chen J, Sinclair G, Rozati H et al (2022) Improving on whole-brain radiotherapy in patients with large brain metastases: a planning study to support the AROMA clinical trial. Radiother Oncol 170:176–183. https://doi.org/10.1016/j.radonc.2022.02.011
3. Tomita N, Kodaira T, Tachibana H et al (2008) Helical tomotherapy for brain metastases: dosimetric evaluation of treatment plans and early clinical results. Technol Cancer Res Treat 7:417–424. https://doi.org/10.1177/153303460800700602
4. Mehta MP, Tsao MN, Whelan TJ et al (2005) The American Society for Therapeutic Radiology and Oncology (ASTRO) evidence-based review of the role of radiosurgery for brain metastases. Int J Radiat Oncol Biol Phys 63:37–46. https://doi.org/10.1016/j.ijrobp.2005.05.023
5. Aoyama H, Shirato H, Tago M et al (2006) Stereotactic radiosurgery plus whole-brain radiation therapy vs stereotactic radiosurgery alone for treatment of brain metastases a randomized controlled trial. JAMA 295:2483–2491. https://doi.org/10.1001/jama.295.21.2483
6. Sanghavi SN, Miranpuri SS, Chappell R et al (2001) Radiosurgery for patients with brain metastases: a multi-institutional analysis, stratified by the RTOG recursive partitioning analysis method. Int J Radiat Oncol Biol Phys 51:426–434. https://doi.org/10.1016/S0360-3016(01)01622-4
7. Brown PD, Ballman KV, Cerhan JH et al (2017) Postoperative stereotactic radiosurgery compared with whole brain radiotherapy for resected metastatic brain disease (NCCTG N107C/CEC·3): a multicentre, randomised, controlled, phase 3 trial. Lancet Oncol 18:1049–1060. https://doi.org/10.1016/S1470-2045(17)30441-2
8. Matsui JK, Perlow HK, Upadhyay R et al (2023) Advances in radiotherapy for brain metastases. Surg Oncol Clin N Am 32:569–586. https://doi.org/10.1016/j.soc.2023.02.007
9. Meniai-Merzouki F, Bernier-Chastagner V, Geffrelot J et al (2018) Hypofractionated stereotactic radiotherapy for patients with intracranial meningiomas: impact of radiotherapy regimen on local control. Sci Rep 8:13666. https://doi.org/10.1038/s41598-018-32124-8
10. Cho B (2018) Intensity-modulated radiation therapy: a review with a physics perspective. Radiat Oncol J 36:1–10. https://doi.org/10.3857/roj.2018.00122
11. De Meerleer GO, Fonteyne VH, Vakaet L et al (2007) Intensity-modulated radiation therapy for prostate cancer: late morbidity and results on biochemical control. Radiother Oncol 82:160–166. https://doi.org/10.1016/j.radonc.2006.12.007
12. Urbano TG, Clark CH, Hansen VN et al (2007) Intensity modulated radiotherapy (IMRT) in locally advanced thyroid cancer: acute toxicity results of a phase I study. Radiother Oncol 85:58–63. https://doi.org/10.1016/j.radonc.2007.07.020
13. Chen WC, Baal UH, Baal JD et al (2021) Efficacy and safety of stereotactic radiosurgery for brainstem metastases: a systematic review and meta-analysis. JAMA Oncol 7:1033–1040. https://doi.org/10.1001/jamaoncol.2021.1262
14. Kron T, Lehmann J, Greer PB (2016) Dosimetry of ionising radiation in modern radiation oncology. Phys Med Biol 61:R167–R205. https://doi.org/10.1088/0031-9155/61/14/r167
15. Guckenberger M, Baus WW, Blanck O et al (2020) Definition and quality requirements for stereotactic radiotherapy: consensus statement from the DEGRO/DGMP working group stereotactic radiotherapy and radiosurgery. Strahlenther Onkol 196:417–420. https://doi.org/10.1007/s00066-020-01603-1
16. Dimitriadis A, Tsang Y, Thomas RAS et al (2020) Multi-institutional dosimetric delivery assessment of intracranial stereotactic radiosurgery on different treatment platforms. Radiother Oncol 147:153–161. https://doi.org/10.1016/j.radonc.2020.05.024
17. Mazaro SJ, Kinoshita A, Nicolucci P et al (2022) Characterization and implementation of the L-alanine detector for quality control of lung SBRT treatments with the VMAT technique. J Radiat Res Appl Sci 15:82–88. https://doi.org/10.1016/j.jrras.2022.01.002
18. Santos T, Ventura T, Capela M et al (2021) A protocol for absolute dose verification of SBRT/SRS treatment plans using GafchromicTM EBT-XD films. Phys Med 82:150–157. https://doi.org/10.1016/j.ejmp.2021.01.082
19. Tuta CS, Amiot MN, Sommier L, Ioan RM (2020) Alanine pellets comparison using EPR dosimetry in the frame of quality assurance for a Gamma Knife system in Romania. Radiat Phys Chem 170:108653. https://doi.org/10.1016/j.radphyschem.2019.108653
20. Yalvac B, Reulens N, Reniers B (2024) Early results of a remote dosimetry audit program for lung stereotactic body radiation therapy. Phys Imaging Radiat Oncol 29:100544. https://doi.org/10.1016/j.phro.2024.100544
21. Albino LD, Cruz ARP, Pieri K et al (2024) Quality control of the stereotactic radiosurgery procedure with the alanine-EPR dosimetry. Radiat Phys Chem 224:112080. https://doi.org/10.1016/j.radphyschem.2024.112080
22. Borca VC, Pasquino M, Russo G et al (2013) Dosimetric characterization and use of GAFCHROMIC EBT3 film for IMRT dose verification. J Appl Clin Med Phys 14:158–171. https://doi.org/10.1120/jacmp.v14i2.4111
23. Shaw M, Lye J, Alves A et al (2021) Characterisation of a synthetic diamond detector for end-to-end dosimetry in stereotactic body radiotherapy and radiosurgery. Phys Imag Radiat Oncol 20:40–45. https://doi.org/10.1016/j.phro.2021.10.002
24. Elter A, Rippke C, Johnen W et al (2021) End-to-end test for fractionated online adaptive MR-guided radiotherapy using a deformable anthropomorphic pelvis phantom. Phys Med Biol 66:245021. https://doi.org/10.1088/1361-6560/ac3e0c

25. Furuya T, Lee YK, Archibald-Heeren BR et al (2020) Evaluation of multi-institutional end-to-end testing for post-operative spine stereotactic body radiation therapy. Phys Imag Radiat Oncol 16:61–68. https://doi.org/10.1016/j.phro.2020.09.005
26. Regulla DF, Deffner U (1982) Dosimetry by ESR spectroscopy of alanine. Int J AppL Radiat Isot 33:1101–1014
27. Marrale M, Longo A, Span M et al (2011) Sensitivity of alanine dosimeters with gadolinium exposed to 6 MV photons at clinical doses. Radiat Res 176:821–826. https://doi.org/10.1667/RR2256.1
28. Baffa O, Kinoshita A (2014) Clinical applications of alanine/electron spin resonance dosimetry. Radiat Environ Biophys 53(2):233–240. https://doi.org/10.1007/s00411-013-0509-2
29. Brai M, Marrale M, Gennaro G et al (2007) Improvement of ESR dosimetry for thermal neutron beams through the addition of gadolinium. Phys Med Biol 52:5219–5230. https://doi.org/10.1088/0031-9155/52/17/008
30. Marrale M, Brai M, Gennaro G et al (2007) Alanine blends for ESR measurements of thermal neutron fluence in a mixed radiation field. Radiat Prot Dosimetry 126:631–635. https://doi.org/10.1093/rpd/ncm128
31. Carlino A, Gouldstone C, Kragl G et al (2018) End-to-end tests using alanine dosimetry in scanned proton beams. Phys Med Biol 63:055001. https://doi.org/10.1088/1361-6560/aaac23
32. Desrosiers MF, Puhl JM (2009) Absorbed-dose/dose-rate dependence studies for the alanine-EPR dosimetry system. Radiat Phys Chem 78:461–463. https://doi.org/10.1016/j.radphyschem.2009.03.025
33. Tsai CL, Wu JK, Chao HL et al (2011) Treatment and dosimetric advantages between VMAT, IMRT, and helical tomotherapy in prostate cancer. Med Dosim 36:264–271. https://doi.org/10.1016/j.meddos.2010.05.001
34. Flatten V, Friedrich A, Engenhart-Cabillic R, Zink K (2020) A phantom based evaluation of the dose prediction and effects in treatment plans, when calculating on a direct density CT reconstruction. J Appl Clin Med Phys 21:52–61. https://doi.org/10.1002/acm2.12824
35. White DR, Booz J, Griffith R V., et al (1989) Report 44 ICRU - 2. Basic Concepts. Reports of the International Commission on Radiation Units and Measurements os-23:3–13. https://doi.org/10.1093/jicru_os23.1.3
36. IAEA (2024) Technical Reports Series No. 398 (Rev. 1). Absorbed Dose Determination in External Beam Radiotherapy. An International Code of Practice for Dosimetry Based on Standards of Absorbed Dose To Water. https://doi.org/10.61092/iaea.ve7q-y94k
37. Marrale M, Abbene L, d'Errico F et al (2017) Characterization of the ESR response of alanine dosimeters to low-energy Cu-target X-tube photons. Radiat Meas 106:200–204. https://doi.org/10.1016/j.radmeas.2017.03.009
38. Ferreira BC, Lopes MC, Capela M (2009) Evaluation of an Epson flatbed scanner to read Gafchromic EBT films for radiation dosimetry. Phys Med Biol 54:1073–1085. https://doi.org/10.1088/0031-9155/54/4/017
39. Niroomand-Rad A, Chiu-Tsao ST, Grams MP et al (2020) Report of AAPM task group 235 radiochromic film dosimetry: an update to TG-55. Med Phys 47:5986–6025. https://doi.org/10.1002/mp.14497
40. Uddin MT (2012) Contributions to the proceedings of IPAC2012. Quality Control of Modern Linear Accelerator: Dose Stability Long and Short-Term. IEEE
41. Marrale M, Longo A, Russo G et al (2015) Dosimetry for electron Intra-operative radiotherapy: comparison of output factors obtained through alanine/EPR pellets, ionization chamber and Monte Carlo-GEANT4 simulations for IORT mobile dedicate accelerator. Nucl Instrum Methods Phys Res B 358:52–58. https://doi.org/10.1016/j.nimb.2015.05.022
42. Sharpe PHG, Sephton JP (1998) alanine dosimetry at NPL-the development of a mailed reference dosimetry service at radiotherapy dose levels. In: International symposium on techniques for high dose dosimetry in Industry, Agriculture and Medicine. Vienna.
43. Hoffmans D, Niebuhr N, Bohoudi O et al (2020) An end-to-end test for MR-guided online adaptive radiotherapy. Phys Med Biol 65:125012. https://doi.org/10.1088/1361-6560/ab8955
44. Takahashi Y, Oshika R, Tachibana R et al (2025) Spatial accuracy of dose delivery significantly impacts the planning target volume margin in linear accelerator-based intracranial stereotactic radiosurgery. Sci Rep 15:3608. https://doi.org/10.1038/s41598-025-87769-z
45. Anton M (2006) Uncertainties in alanine/ESR dosimetry at the Physikalisch-Technische Bundesanstalt. Phys Med Biol 51:5419–5440. https://doi.org/10.1088/0031-9155/51/21/003
46. Schaeken B, Cuypers R, Lelie S et al (2011) Implementation of alanine/EPR as transfer dosimetry system in a radiotherapy audit programme in Belgium. Radiother Oncol 99:94–96. https://doi.org/10.1016/j.radonc.2011.01.026